INTERNATIONAL JOURNAL OF HYDROGEN ENERGY 40 (2015) 16892–16900

Available online at www.sciencedirect.com

ScienceDirect

journal homepage: www.elsevier.com/locate/he

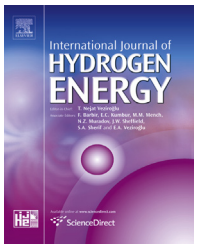

Hydrogen embrittlement in nickel, visited by first principles modeling, cohesive zone simulation and nanomechanical testing

A. Alvaro [a,*], I. Thue Jensen [b], N. Kheradmand [c], O.M. Løvvik [b], V. Olden [a]

[a] SINTEF, Materials and Chemistry, Richard Birkelands v. 2b, 7465 Trondheim, Norway
[b] SINTEF, Materials and Chemistry, Forskningsveien 1, 0314 Oslo, Norway
[c] NTNU, Department of Engineering Design and Materials, Richard Birkelands v. 2b, 7465 Trondheim, Norway

ARTICLE INFO

Article history:
Received 29 October 2014
Received in revised form
24 May 2015
Accepted 2 June 2015
Available online 9 July 2015

Keywords:
Hydrogen
Nickel
Embrittlement
Multiscale modeling
Grain boundary
Nanomechanical testing

ABSTRACT

Hydrogen (H) can have dramatic consequences on material properties, especially by reducing the fracture toughness. Degradation by H initiates through mechanisms at the nano-scale, and is normally not detectable prior to the final leakage or component fracture. Computational techniques are therefore being developed in order to provide both a wider understanding of the phenomenon and engineering tools for prediction of materials susceptibility toward hydrogen embrittlement. This work presents a preliminary study for the development of a novel computational approach in which density functional theory (DFT), nanoscale experiments and finite element (FE) modeling are combined and interrelated in order to improve the understanding of hydrogen induced intergranular cracking. Two low angle and low coincidence grain boundaries types have been considered: Σ_3 and Σ_5. Density Functional Theory has been applied to investigate the influence of an increasing number of H atoms on the cohesive strength of these grain boundaries in pure Nickel. This provided relations between the number of H atoms (coverage of the grain boundary) and the cohesive strength, which is further applied in cohesive zone FE modeling of a triangular nanometer sized fracture mechanics cantilever beam. For verification of the model such specimens will be tested experimentally both with and without in-situ electrochemical charging.

The simulation results show that the model is suitable for describing the combined effect of grain boundary misorientation and the reduced cohesive energy due to hydrogen on the grain boundary propensity to cleave.

Introduction

Stress corrosion cracking (SCC) and hydrogen embrittlement (HE) are threats to the structural integrity of offshore oil and gas pipelines and components and can cause costly downtime and repair. The main source of atomic hydrogen (H) in oil & gas fields is the corrosion protection systems, where H is formed at the cathode at normal protection potentials and enters the steel by absorption. Another source may be welds,

* *Corresponding author*. Tel.: +47 96 73 84 51.
E-mail address: antonio.alvaro@sintef.no (A. Alvaro).
http://dx.doi.org/10.1016/j.ijhydene.2015.06.069

caused by the presence of moisture during repair welding. Lately, there are reports about the tendency of premature failure of materials despite being considered "safe" considering the design criteria and resistance towards HE (*e.g.* super duplex stainless steel (SDSS) and nickel-base alloys) [1,2].

Modern steels are designed on the basis of introduction of different interfaces into the microstructure and reduction of the grain size. It is already known that grain boundary (GB) density, as well as their types and misorientation, play a fundamental role in the macro-behavior of polycrystalline metallic materials, including the resistance to crack nucleation and propagation [3,4]. On the other hand, interfaces and grain boundaries may act as preferential sites for trapping and segregation for H atoms, finally leading to intergranular embrittlement and cracking. In the case of aging offshore steel infrastructure the role of the grain boundaries and interfaces become more important since these traps are potential initiation sites for failure as well as sources of H to the failure sites through high diffusion rate paths. While hydrogen embrittlement is a well-known phenomenon, the mechanisms involved are still not fully understood. Two of the most established micromechanical models of hydrogen-assisted fracture are the hydrogen enhanced decohesion model (HEDE) [5–8] and the hydrogen enhanced local plasticity model (HELP) [9–11]. Adsorption induced dislocation emission (AIDE) [12] and the thermodynamic framework of Defactant concept proposed by Kirchheim [13] are others. Recently it has been shown that quantum effects need to be considered in order to achieve a correct understanding of the degradation mechanisms in construction materials [14,15].

A logical approach for understanding the hydrogen effect on the GB under stress is to study the mechanical behaviour of bi-crystal cantilevers, containing a single defined GB [16]. Bicrystalline cantilevers including one single predefined interface is prepared by means of focused ion beam (FIB). With the application of cathodic polarization it is possible to charge the cantilevers with H. The small size of the cantilevers assures a uniform concentration of H and fast saturation of the GB with H. The results can then be compared to similar cantilevers deformed in H free condition. This makes it possible to quantify and verify the effect of H on the interface cohesion energy.

The work presented is preliminary in nature: the main goal is to investigate and evaluate the suitability of the proposed multiscale modelling approach for providing a better understanding of hydrogen induced GB separation as well as a tool for experimental design. Density functional theory is applied to investigate the influence of different levels of atomic H on the cohesive strength and embrittlement mechanism involving grain boundaries and interfaces. Input from atomistic modeling provides quantitative information to cohesive zone (CZ) elements, implemented in the FE code ABAQUS. The cohesive elements are placed between grains which are consistently oriented in order to represent specific GB on a continuum level. The critical energy for the collapse of the element is therefore linked to the H coverage of the GB. Finally, the procedure is applied for the simulation of nanometer sized fracture mechanics cantilever beams of a Nickel bi-crystal.

Materials and methods

Nickel is the simplest relevant model system to establish the basic methodology and competence before establishing projects on more industrial relevant alloys.

Bulk samples in form of thin discs with 10 mm diameter and 2 mm thickness were prepared from as-received 99.99% pure Nickel according to the description in Ref. [17] to produce two dimensional samples, i.e. the GB perpendicular to the sample surface, so that any geometrically-caused parameters affecting the results will be excluded. The discs were characterized using electron backscatter diffraction (EBSD) to verify the GB types and then electro polished to prepare a perfectly clean surface.

Cantilevers with 4 μm length and 2 μm width were milled using a FEI Helios NanoLab 600 DualBeam FIB. Milling of cantilevers was performed in two steps: first a balk roughly to the final length and width of the cantilever was milled using 30 kV and 0.9 pA beam current (Fig. 1a). Next the balk was milled from the sides by rotating 90° to release it from the bulk sample. and milled from both sides within rotating by 180° (Fig. 1b). In this second step the FIB stage was tilted back to 7°, and so the cross section of the cantilever became a triangle with an angle of 45° (Fig. 1c). This step is also called fine milling step using lower voltage of 10 kV and current of 0.2 pA. In this way, the damaged layer in the first step by the high voltage/current is removed for the most part. The GB was located at the one fourth total length of the cantilever from the cantilever end.

Prepared cantilevers will be tested under bending test in air and in the hydrogen contained atmosphere, which will be presented in upcoming reports. As an ongoing study, this part was presented to show that by performing experimental tests, we verify our simulation studies.

Theory and calculations

Input from existing atomic scale modeling such as the work of Jiang et al. [18] has already been used in the past [19,20] to improve the predictive capacity of continuum models. In this work, however, the aim is to set up a framework in which atomic scale experiments and modeling are tailor-made to answer challenges faced at the continuum and FE level.

Atomistic level – DFT

Spin polarized DFT calculations at the PBE-GGA level [21] were performed for Ni $\Sigma_5(012)$ and $\Sigma_3(111)$ symmetrical grain boundaries (GBs) using the Vienna ab-initio simulation package (VASP) [22,23]. The criterion for energy convergence was a change of the total energy less than 10^{-5}. The plane-wave energy cut-off was 450 eV and a $7 \times 7 \times 3$ Gamma sampling of k-points was used to model the Brillouin zone. The energy cut-off and k-points were tested by comparing the energy of models with one and two hydrogen atoms. The chosen values gave relative energy convergences better than 1 meV. The closed GB unit cells consisted of 80 and 96 Ni atoms as illustrated in Fig. 2, into which an increasing amount of H was

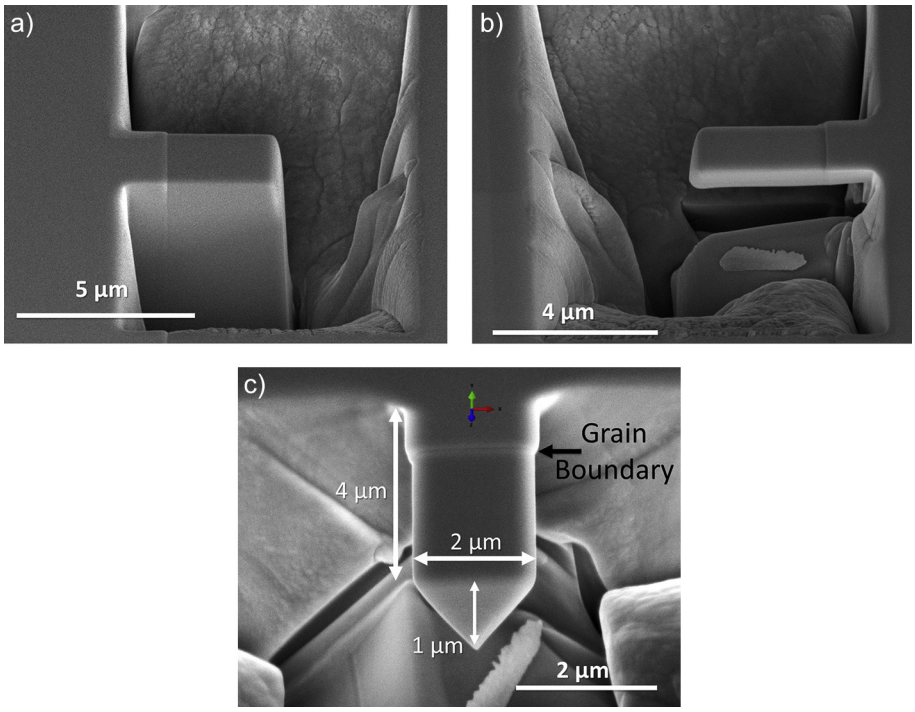

Fig. 1 – a) Milling a balk roughly the same size of the final cantilever using high beam voltage/current. b) Balk milled from both sides, by rotating 180°. c) Bicrystalline cantilever with the final shape and size; the reference system at the cantilever end refers to the FE simulation global system.

added. Such unit cells have to contain two GBs in order to preserve periodicity. To simulate a crack the interfaces of the middle GB was separated by a vacuum layer of 15 Å, which was considered long enough to avoid any interactions between the two surfaces. H was introduced into different interstitial sites in the system to check which ones were preferred.

Structural optimizations were performed, where atomic positions and lattice parameters where allowed to change freely for the uncracked models. For the cracked model only the atomic positions were allowed to relax. The break condition for the relaxation loop was set to forces < -0.01 eV/Å. The formation enthalpy of the model was calculated as follows:

$$\Delta H_f = E_{Ni(GB)+xH} - E_{Ni(fcc)} - \frac{x}{2}E_{H_2(gas)} \quad (1)$$

where $E_{Ni\ (GB)+xH}$, $E_{Ni(fcc)}$ and $E_{H2(gas)}$ are the calculated energies of the GB system with x H atoms, pure Ni without GB, and H_2 gas, respectively. Decohesion was investigated by comparing the total energy of the cracked and uncracked models for each H content. The ideal fracture energy (2γ) [18] was defined as follows:

$$2\gamma = \frac{E_{GB+xH}^{cracked} - E_{GB+xH}^{uncracked}}{2A} \quad (2)$$

where $E_{GB+xH}^{uncracked}$ and $E_{GB+xH}^{cracked}$ are the calculated energies of the GB system with x H atoms before and after cracking and A is the area of the GB plane, i.e., $2A$ is the area of the surfaces created by the crack. The ideal fracture energy as function of H coverage (Θ_H), intended as the ratio of the sites actually occupied by hydrogen and the total number of sites available for occupancy [24], was given as input for the FE calculations.

Continuum level – cohesive zone modelling

On the continuum scale, the nanosize bi-crystal cantilever beam is modelled by using the finite element code ABAQUS. Since the macroscopic elastic behaviour of face-centered cubic (FCC) bi-crystal nickel is affected by the crystallographic orientation of the single grain [25], the current material model is defined as fully elastic and anisotropic, i.e. in the most general definition, 36 components C_{ij} for the elastic constant matrix C are needed to fully describe the mechanical behaviour of the material. However, by taking advantage of the symmetry properties of the stiffness matrices ($C_{ij=}\ C_{ji}$) and that of the cubic crystal structures, the number of independent elastic constant is reduced to three C_{11}, C_{12} and C_{44}., as given in (3):

$$C = \begin{bmatrix} C_{11} & C_{12} & C_{12} & & & \\ C_{12} & C_{11} & C_{12} & & & \\ C_{12} & C_{12} & C_{11} & & & \\ & & & C_{44} & & \\ & & & & C_{44} & \\ & & & & & C_{44} \end{bmatrix} \quad (3)$$

Here C_{11}, C_{12} and C_{44} are equal to 244 GPa, 158 GPa and 102 GPa, respectively, as calculated by Wen et al. [26].

The misorientation between the two grains is described by Euler angles in Bunge definition, i.e. extrinsic ZXZ convention, as shown schematically in Fig. 3, while a list of the different angles values in extrinsic ZXZ convention for Σ_3 to Σ_{11} configurations are summarized in Table 1.

The GB is represented by cohesive elements whose scope is to handle the material damage. Cohesive elements can be imagined as two faces of initial thickness close to zero. They

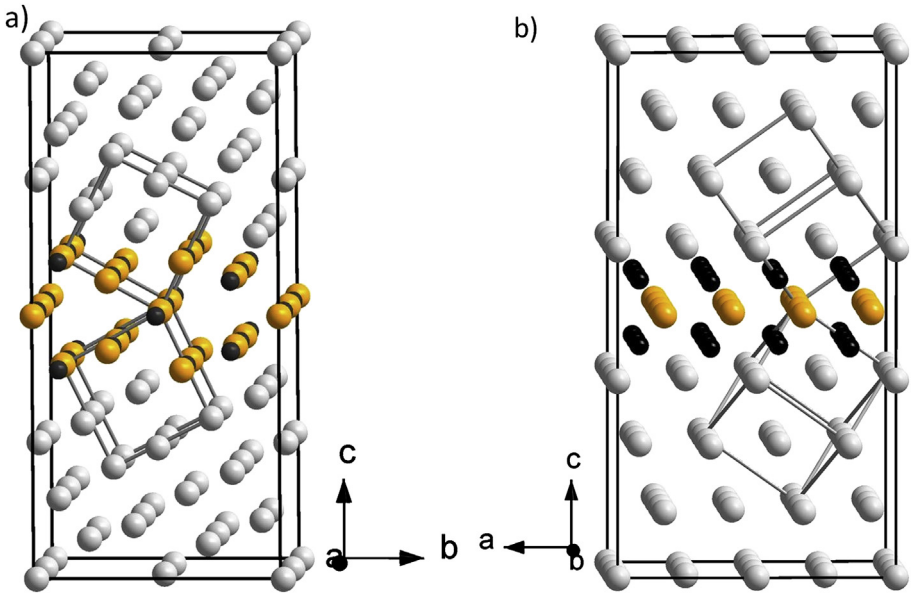

Fig. 2 – a) The Σ_5(012) and b) Σ_3(111) GB models used in the DFT calculations. Small dark balls represent H atoms. Large white balls represent Ni atoms with bulk Ni coordination, while large darker (orange) balls represent Ni atoms with coordination altered by the GB. The orientation of the bulk Ni *fcc* unit cell is shown for each GB. (For interpretation of the references to colour in this figure legend, the reader is referred to the web version of this article.)

are placed between and share nodes with the adjacent continuum elements which represent the two nickel crystals. Their behaviour is determined by a traction separation law (TSL) which defines their constitutive behaviour in all element directions.

With increasing interfacial separation, the traction across the newly created interfaces reaches a maximum (damage initiation point) and then decreases until the maximum separation is reached, allowing complete decohesion [27]. In this preliminary work, a simple bi-linear TSL is used, as showed in Fig. 4. The maximum nominal stress criterion in ABAQUS is adopted, meaning that damage is initiated as soon as the opening stress in any of the three directions overcomes the maximum at the damage initiation point. In this study the damage initiation point is chosen as three times the yield strength of pure nickel, i.e. 525 MPa [28]. Finally the cohesive energy, which is visualized by the area enveloped by the TSL, is considered to represent the GB separation energy as obtained from the DFT simulations. A particular mention needs to be made with regards to the elastic cohesive stiffness, indicated by K_n in Fig. 4. The values of K_n, which are also connected to the initial thickness of the cohesive elements, should always be higher than the Young modulus E of the surrounding material [20] and, at the same time, low enough to avoid convergence problems [29]. In this study, a ratio K_n/E of 20 has been found to give the best compromise.

A description of the FE-model framework is presented in Fig. 5. Grain 1 and Grain 2 are modelled by hexahedral cubic elements C3D8R while the GB, which is placed at ¼ of the total cantilever length from the plane of encastre, is represented by a plane of consistently oriented cohesive elements COH3D8. The length of the triangular cantilever beam is 4 μm, the base and the height of the triangular section are 2 μm and 1 μm, respectively, in order to mirror the dimensions as given in Fig. 1. A preliminary study of the proposed model is made on Σ_3 and Σ_5 GB types. The material orientations for Σ_3-type and mechanical boundary conditions are also reported in Fig. 5. Finally, the load is applied as a negative displacement of 0.2 μm along the y-axis. The force at the cantilever end is obtained as the sum of the reaction forces along the y-direction of the encastred nodes.

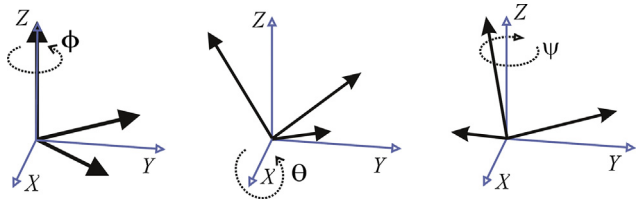

Fig. 3 – Schematic representation of Euler angles in extrinsic ZXZ convention.

Table 1 – Angle values in degrees for different Coincident Lattices Sites Σ configurations. Angles refers to the extrinsic ZXZ convention represented in Fig. 1.

CLS	Φ	Θ	Ψ
Σ_3	45	70.53	45
Σ_5	0	90	36.86
Σ_7	26.56	73.4	63.44
Σ_9	26.56	83.62	26.56
Σ_{11}	33.68	79.53	33.68

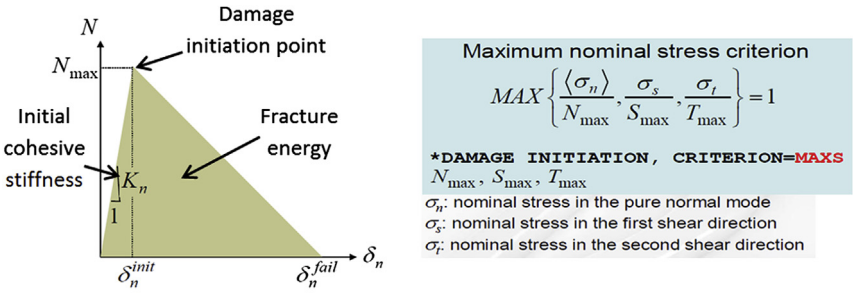

Fig. 4 – Bilinear traction separation law and the maximum nominal stress criterion for damage initiation as defined by ABAQUS [25].

Results and discussion

For the Σ_5(012) model the DFT calculations clearly show that H prefers octahedral-like positions similar to the ones found in bulk Ni, rather than the position in the middle of the void. The position in the middle of the void is preferred for larger impurities, *e.g.* sulfur [30]. This results in a total of 20 GB sites for H around the voids created by the GB in the Σ_5 (012) model, as illustrated in Fig. 2. The octahedral-like positions are also preferred in the Σ_3(111) model, resulting in a plane of 12H atoms on one side of the GB itself, as illustrated in Fig. 1.

Fig. 6 shows relative formation energy of the Σ_5(012) and Σ_3(111) models, comparing the energy cost of having the hydrogen in the GB model compared to having H in bulk Ni or in gas form. In Fig. 6a it is clearly shown that the Σ_5(012) GB will attract H both from H_2 gas and from bulk Ni, indicating that the Σ_5(012) GB is exposed to accumulation of H both from outside and inside the material. For Σ_3(111) on the other hand, it is different. As shown in Fig. 6b) the Σ_3(111) GB does not seem to attract H at all from H_2 gas and bulk Ni with low H content. However, once the H content exceeds a certain amount, the H affinity of the GB sites starts to increase with increasing H content. We attribute this to the fact that the Σ_3(111) GB can be compared to a minimal defect in bulk Ni. While the Σ_5(012) GB creates imperfections in the crystal structure which H can help relax, introducing H into the Σ_3(111) GB serves more to create imperfections than to mend them. Thus the result of adding H into the Σ_3(111) GB is to create defects, which at a certain point will make it beneficial to add even more H to relax the tension caused by the imperfections initially imposed. Hence, the negative slope in Fig. 6b can be explained, but we think it represents a purely hypothetical case, as it is unlikely to ever see this kind of H accumulation in a Σ_3(111) GB in a real Ni system, unless perhaps if the material is intentionally charged with H.

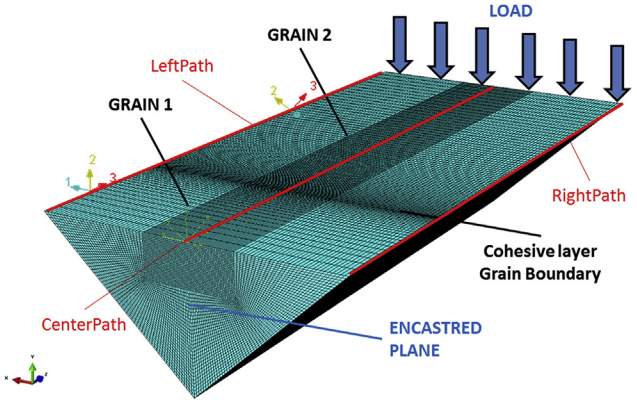

Fig. 5 – FE model of the nanosize cantilever beam. Grains orientation for a Σ_3 grain boundary is indicated as well as the mechanical boundary conditions for the simulations.

Fig. 7 shows the calculated ideal fracture energies as function of the hydrogen coverage. The values for the Σ_5(012) and Σ_3(111) GBs are compared to fracture along the corresponding planes in bulk Ni. Results indicate Σ5(012) GB as the weakest of the investigated GB models, which also exhibit a significant reduction of strength compared to the 012 plane in bulk Ni. As one could expect, there is minimal effect of the Σ_3(111) GB compared to the 111 plane in bulk Ni.

Results from ABAQUS cohesive simulations are summarized in Figs. 8–10 and they summarize the combined influence of the misorientation and the first principle cohesive energy on the mechanical response of the bi-crystal system. Fig. 8 presents a plot of load vs vertical displacement of the cantilever beam for the Σ_3 and Σ_5 misorientation. For the sake of clarity, simulated separation energy results for zero and full hydrogen coverage are presented for each type of misorientation. From a general point of view, Σ_3 misorientation provides a higher resistance to fracture than Σ_5 (see Fig. 8), both when the cohesive energy levels correspond to hydrogen coverage of 0 and 100%. These results descend from two main contributions: the different fracture energies obtained from atomistic simulations on one side and the effect of the different crystal misorientation on the mechanical response of the whole cantilever beam, on the other. This is further confirmed by analyzing the plots in Figs. 9 and 10. Fig. 9 shows the different ways in which the GB disbonding happens as a function of GB type and the hydrogen coverage. Each of the plots in Fig. 9 presents the cohesive elements appearance which refers to a particular stage during the simulation indicated by the blue and red numbered boxes in Fig. 8. For instance, Fig. 9c refers to simulations of Σ_3 coincidence GB, with full hydrogen coverage (as indicated in the text box next to the plot MaxH) and refers to the simulation point indicated by the blue square numbered with 3 in Fig. 9

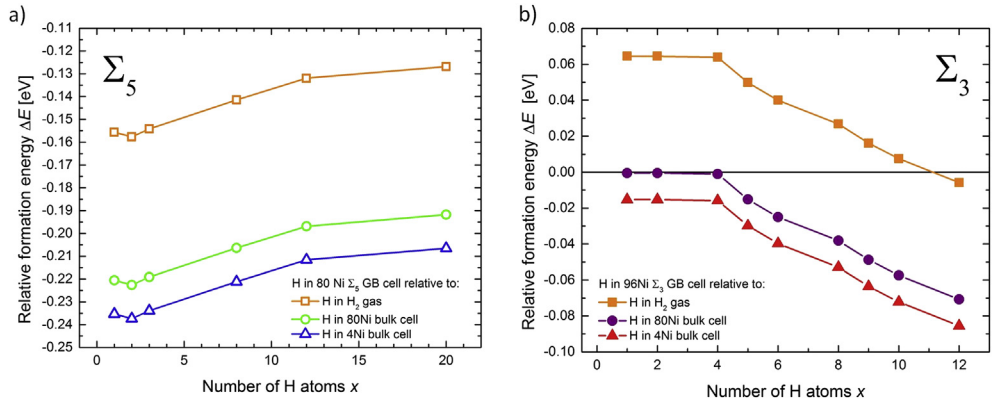

Fig. 6 – The energy cost of *x* H atoms in a) $\Sigma_5(012)$ and b) $\Sigma_3(111)$ GB models relative to $\frac{x}{2}$ H in H_2 gas (squares), *x* times 1H in an 80 Ni bulk cell (circles), and *x* times 1H in a 4Ni bulk cell (triangles). Negative values mean that the GB model is the favored state. Lines are included as guide for the eyes.

(Blue3). This type of analysis shows that the opening of the cohesive layer between the grains in Σ_3 configuration happens in a coherent way from the top through the bottom of the triangular section of the cantilever beam, almost as no misorientation is present (see Fig. 9a and b for hydrogen free cohesive energies and 9c and 9d for 100% hydrogen coverage cohesive energy.). The effect of the misorientation on the stress distribution (plotted in Fig. 10) at the boundary and, consequently, on the "shape" of the separation/fracture of the cohesive layer is evident from the results for the Σ_5 configuration. In this configuration, fracture starts from the left top side of the cantilever beam and proceeds toward the bottom tilted with an angle of approximately 15–20° (see Fig. 9e and f). It is interesting to note that this angle tend to increase for the simulations performed with 100% hydrogen coverage (see Fig. 9g and h).

Finally, in Fig. 10, the opening stress (in this case σ_{33}) is plotted along three paths, called LeftPath, CenterPath and RightPath in Fig. 5, at one increment before the damage initiation point is reached. It is evident how, for the Σ_3 configuration, the opening stress develops symmetrically with respect to the central longitudinal section of the triangular beam while this is not the case for Σ_5 configuration.

Conclusions & further work

This work provided preliminary results on the suitability of the proposed multiscale modeling approach for describing and, eventually, providing a reliable tool for the prediction of intergranular fracture in presence of hydrogen. The model was built to simulate the mechanical response in a nanosized nickel bi-crystal cantilever beams with full H-coverage and in H-free conditions. Despite it has been recently showed that low Σ coincidence boundaries are almost immune to intergranular fracture [3,4], Σ_3 and Σ_5 coincidence GB types were chosen for a qualitative analysis.

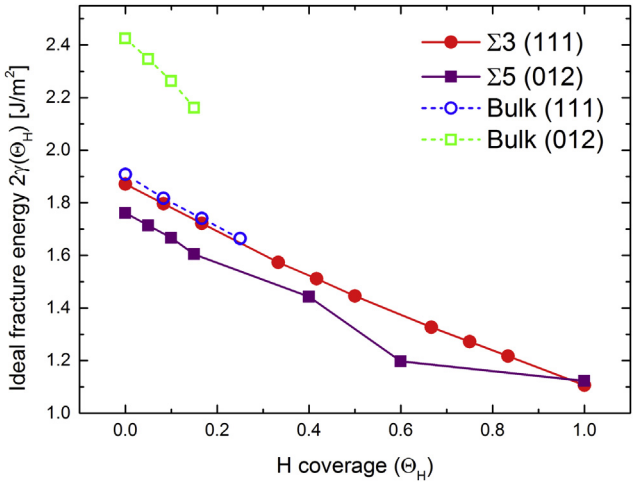

Fig. 7 – Ideal fracture energy as function of H coverage for the $\Sigma_5(012)$ (solid squares) and $\Sigma_3(111)$ (solid circles) GB models. Open symbols show results for the corresponding bulk planes. Lines are included as guide for the eyes.

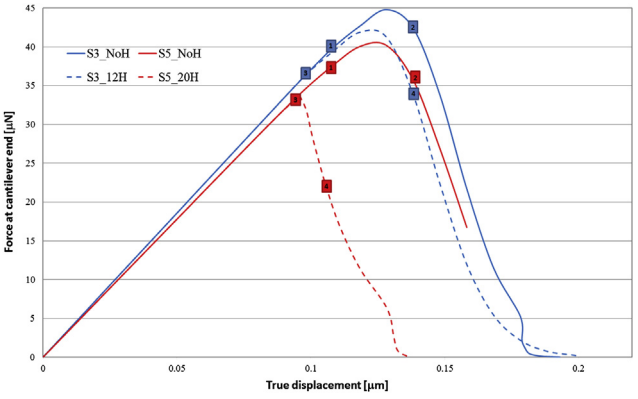

Fig. 8 – Force vs. displacement plots of bi-crystal cantilever beam for Σ_3 (blue lines) and Σ_5 (red lines) misorientation types. Solid lines: 0%-hydrogen coverage cohesive energies; dotted lines: 100% hydrogen coverage cohesive energies. (For interpretation of the references to colour in this figure legend, the reader is referred to the web version of this article.)

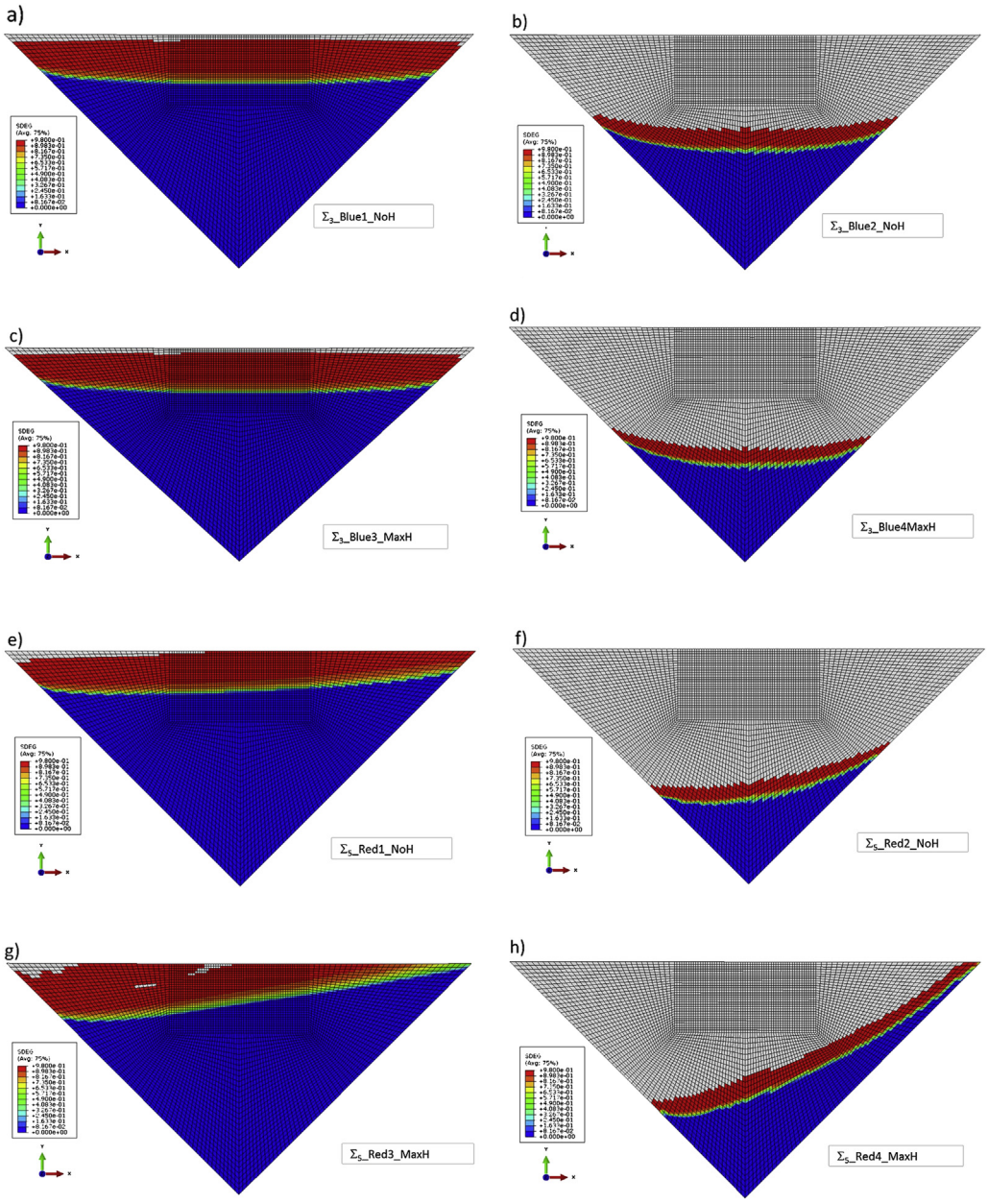

Fig. 9 – Cohesive elements status of degradation (SDEG) resulting from the different simulations. In the text box next to each figure it is indicated the stage of the simulation to which it refers to. For instance, Fig. 9c refers to simulations of Σ_3, 100% hydrogen coverage cohesive energy (MaxH) and refers to the point blue square 3 in Fig. 9 (Blue3). (For interpretation of the references to colour in this figure legend, the reader is referred to the web version of this article.)

The main results can be summarized as follows:

- The presented model was able to describe the combined influence of GB misorientation and hydrogen presence on the mechanical response of the bi-crystal system.
- On the atomistic scale, hydrogen and the specific GB misorientation significantly influenced the fracture energies. In particular, the Σ_5(012) GB was more susceptible than the Σ_3(111) GB models.
- The Σ_3(111) GB showed negligible reduction in decohesion strength due to hydrogen compared to the (111) plane in bulk Ni whereas the Σ_5(012) GB resulted in a strong reduction; about 40% of the strength compared to the (012) plane in bulk Ni.
- The effect of the GB misorientation plays an important role in the stress field distribution in the cantilever and strongly affects the fracture process of the cohesive element layer: for Σ_3 the fracture proceeds gradually from the top towards the bottom of the beam section. For the Σ_5 coincidence GB the fracture starts from the left top side of the cantilever beam and proceeds toward the bottom tilted with an angle of approximately 15–20°.

The presented work should be regarded as a preliminary. Ongoing and further work:

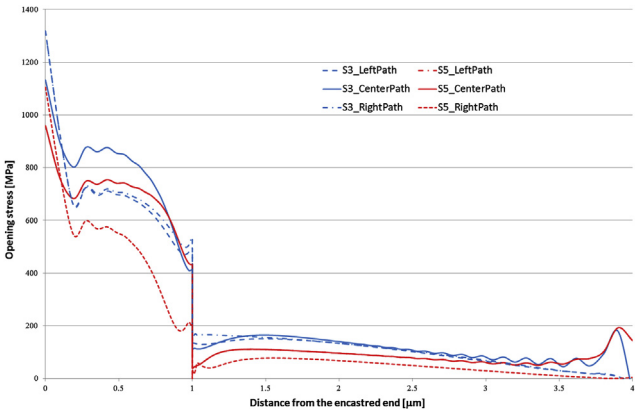

Fig. 10 – Plots of the variation of the opening stresses along the three path defined in Fig. 5 for Σ_3 (blue lines) and Σ_5 (red lines) misorientation types. The plots are taken one increment before damage initiation point is reached. (For interpretation of the references to colour in this figure legend, the reader is referred to the web version of this article.)

- On atomistic scale: The determination of the number of GB sites, which represents full H coverage ($\Theta_H = 1$), is part of an ongoing investigation of the effect of unit cell size and relaxation procedures.
- Development of a procedure that creates ad-hoc real grain boundaries by directly transferring information from EBSD analysis.
- Quantitative verification of the model through nano-mechanical testing of the cantilever beam with in-situ charging.
- 3D user defined hydrogen influenced cohesive elements have been used by the authors in previous works [20,31]. Implementation of these elements into this model framework is ongoing.
- An additional crystal plasticity model framework will be developed and implementation in order to account for the influence of plastic strain on hydrogen diffusion and GB segregation.

Acknowledgments

This work has been funded by the Research Council of Norway (Petromaks2 programme, Project no. 234130, HIPP) and by SINTEF as part of the internal strategic research program SEP. The authors also wish to thank Prof. Afroz Barnoush and Dr. Amin Azar for providing valuable advices and challenging discussions during the development of the research.

REFERENCES

[1] Jackson HF, Nibur K, San Marchi C, Puskar J, Somerday B. Hydrogen-assisted crack propagation in 304L/308L and 21Cr–6Ni–9Mn/308L austenitic stainless steel fusion welds. Corros Sci 2012;60:136–44.
[2] Von der Ohe C, Johnsen R, Espallargas N. Multi-degradation behavior of austenitic and super duplex stainless steel–The effect of 4-point static and cyclic bending applied to a simulated seawater tribocorrosion system. Wear 2012;288:39–53.
[3] Watanabe T. Structural effects on grain boundary segregation, hardening and fracture. Le J De Physique Colloques 1985;46(C4). C4-555–C4-566.
[4] Lim L, Watanabe T. Fracture toughness and brittle-ductile transition controlled by grain boundary character distribution (GBCD) in polycrystals. Acta Metall Mater 1990;38:2507–16.
[5] Troiano A. The role of hydrogen and other interstitials in the mechanical behavior of metals (Edward de Mille Campbell memorial Lecture). Trans ASM 1960;52:147–57.
[6] Oriani R. The diffusion and trapping of hydrogen in steel. Acta Metall 1970;18:147–57.
[7] Gerberich WW, Marsh P, Hoehn J. Hydrogen induced cracking Mechanisms—Are there critical experiments? hydrogen effects in materials. Warrendale, PA: The Minerals, Metals, and Materials Society; 1994. p. 539–51.
[8] Vehoff H, Rothe W. Gaseous hydrogen embrittlement in FeSi- and Ni-single crystals. Acta Metall 1983;31:1781–93.
[9] Birnbaum H, Sofronis P. Hydrogen-enhanced localized plasticity-a mechanism for hydrogen-related fracture. Mater Sci Eng A 1994;176:191–202.
[10] Liang Y, Sofronis P. Toward a phenomenological description of hydrogen-induced decohesion at particle/matrix interfaces. J Mech Phys Solids 2003;51:1509–31.
[11] Delafosse D, Magnin T. Hydrogen induced plasticity in stress corrosion cracking of engineering systems. Eng Fract Mech 2001;68:693–729.
[12] Lynch S. A fractographic study of gaseous hydrogen embrittlement and liquid-metal embrittlement in a tempered-martensitic steel. Acta Metall 1984;32:79–90.
[13] Kirchheim R. On the solute-defect interaction in the framework of a defactant concept. Int J Mater Res 2009;100:483–7.
[14] Proville L, Rodney D, Marinica M-C. Quantum effect on thermally activated glide of dislocations. Nat Mater 2012;11:845–9.
[15] Song J, Curtin W. Atomic mechanism and prediction of hydrogen embrittlement in iron. Nat Mater 2013;12:145–51.
[16] Kheradmand N, Barnoush A, Vehoff H. Investigation of the role of grain boundary on the mechanical properties of metals. J Phys Conf Ser 2010:012017. IOP Publishing.
[17] Kheradmand N, Vehoff H, Barnoush A. An insight into the role of the grain boundary in plastic deformation by means of a bicrystalline pillar compression test and atomistic simulation. Acta Mater 2013;61:7454–65.
[18] Jiang D, Carter E. First principles assessment of ideal fracture energies of materials with mobile impurities: implications for hydrogen embrittlement of metals. Acta Mater 2004;52:4801–7.
[19] Olden V, Thaulow C, Johnsen R, Østby E, Berstad T. Application of hydrogen influenced cohesive laws in the prediction of hydrogen induced stress cracking in 25% Cr duplex stainless steel. Eng Fract Mech 2008;75:2333–51.
[20] Alvaro A, Olden V, Akselsen OM. 3D cohesive modelling of hydrogen embrittlement in the heat affected zone of an X70 pipeline steel–Part II. Int J Hydrogen Energy 2014;39:3528–41.
[21] Perdew JP, Chevary J, Vosko S, Jackson KA, Pederson MR, Singh D, et al. Atoms, molecules, solids, and surfaces: Applications of the generalized gradient approximation for exchange and correlation. Phys Rev B 1992;46:6671.

[22] Kresse G, Furthmüller J. Efficient iterative schemes for ab initio total-energy calculations using a plane-wave basis set. Phys Rev B 1996;54:11169.
[23] Kresse G, Furthmüller J. Efficiency of ab-initio total energy calculations for metals and semiconductors using a plane-wave basis set. Comput Mater Sci 1996;6:15–50.
[24] Serebrinsky S, Carter E, Ortiz M. A quantum-mechanically informed continuum model of hydrogen embrittlement. J Mech Phys Solids 2004;52:2403–30.
[25] Den Toonder J, Van Dommelen J, Baaijens F. The relation between single crystal elasticity and the effective elastic behaviour of polycrystalline materials: theory, measurement and computation. Model Simul Mater Sci Eng 1999;7:909.
[26] Wen M, Barnoush A, Yokogawa K. Calculation of all cubic single-crystal elastic constants from single atomistic simulation: hydrogen effect and elastic constants of nickel. Comput Phys Commun 2011;182:1621–5.
[27] ABAQUS. Version 6.13. Analysis users'manual. ABAQUS Inc.; 2013.
[28] Polák J, Milne I, Ritchie RO, Karihaloo B. Comprehensive structural integrity. Amsterdam, London: Elsevier; 2003.
[29] Diehl T. On using a penalty-based cohesive-zone finite element approach, Part I: elastic solution benchmarks. Int J Adhesion Adhesives 2008;28:237–55.
[30] Yamaguchi M, Shiga M, Kaburaki H. Grain boundary decohesion by impurity segregation in a nickel-sulfur system. Science 2005;307:393–7.
[31] Alvaro A, Olden V, Akselsen OM. 3D cohesive modelling of hydrogen embrittlement in the heat affected zone of an X70 pipeline steel. Int J Hydrogen Energy 2013;38(18):7539–49.